

# Constraining the nuclear matter equation of state around twice saturation density

A. Le Fèvre<sup>a</sup>, Y. Leifels<sup>a</sup>, W. Reisdorf<sup>a</sup>, J. Aichelin<sup>b</sup>, Ch. Hartnack<sup>b</sup>

<sup>a</sup>*GSI Helmholtzzentrum für Schwerionenforschung GmbH, Darmstadt, Germany*

<sup>b</sup>*SUBATECH, UMR 6457, Ecole des Mines de Nantes - IN2P3/CNRS - Université de Nantes, France*

---

## Abstract

Using FOPI data on elliptic flow in Au+Au collisions between 0.4 and 1.5A GeV we extract constraints for the equation of state (EOS) of compressed symmetric nuclear matter using the transport code IQMD by introducing an observable describing the evolution of the size of the elliptic flow as a function of rapidity. This observable is sensitive to the nuclear EOS and a robust tool to constrain the compressibility of nuclear matter up to  $2 \rho_0$ .

*Keywords:*

heavy ions, elliptic flow, nuclear equation of state

*PACS:* 25.75.-q, 25.75.Dw, 25.75.Ld

---

## 1. Introduction

The equation of state (EOS) of nuclear matter is of fundamental interest and has been the object of intense theoretical efforts since several decades. The interest is boosted by the fact that it is an important ingredient in modeling fascinating astrophysical phenomena such as compact stars [1] and core collapse supernovae [2]. The calculation of the nuclear EOS from first principles, such as very recently attempted in [3], is a very complex task.

The theory of nuclear forces, such as reviewed in [4], requires a confrontation with empirical facts, when it is applied to the 'ab initio' problem of EOS calculations. In the last decade astrophysicists have pointed out (for a recent review, see [1]) that the EOS relevant for compact stars can in principle be deduced from the increasingly accurate and voluminous systematics of 'neutron' star masses and radii by use of the relativistic Tolman-Volkov-Oppenheimer (TOV) equations. However, at the present time precise model-independent radii are still missing [5], while on the mass front line considerable progress has been made [6, 7]. Nevertheless the need of additional information remains: the composition of matter in the core of neutron stars is not known so far.

A complementary method to approach the nuclear equation of state, practiced since the mid-eighties, is the use of heavy ion collisions over a wide range of incident energies, system sizes and compositions. The general difference between astrophysical and earth bound experiments is that the latter ones deal with rather isospin symmetric ( $N \approx Z$ ,  $N$  neutron,  $Z$  proton number) system compositions than are expected in the center of compact stars, and also, presumably, the temperatures in such reactions are much higher. There are, besides astrophysics, very good reasons to study symmetric (or almost symmetric) nuclear matter. It is clear that we must understand symmetric nuclear matter if we want to explain the properties of nuclei. Convincing theories are expected to reproduce properties of symmetric and 'pure' (or 'almost pure') neutron matter on the same footing. Also the

possibility of a phase transition as the density/temperature is raised can only be studied quantitatively in heavy ion reactions.

However, deriving constraints on the nuclear equation of state (EOS) from heavy-ion collision data is a highly non-trivial task: we are in a dynamic situation with the characteristics describing the state of the system varying rapidly in time, while the observables are measured long after the various incoming and created parts of the system have separated forming a three-dimensional momentum pattern filling large (but not all) parts of phase space. Clearly, the claim to a significant 'constraint' on the EOS cannot easily be made 'model-independent'.

So far attempts to derive reasonably narrow constraints are limited to the energy regime below 10A GeV. The reason is that exclusively for this energy regime some kind of a clock is available. As described in a short, but pedagogical description [8] of the reaction scenario in this regime, a clock is provided by the fact that the 'spectator' nucleons, not initially hit in collisions with non-zero impact parameters, are in contact with the more central 'participant' matter that forms the compressed 'fireball' for a defined time, the passing time, or "blockage time" [8]. This time turns out to be comparable to the expansion time. The latter is governed by a fundamental property, the sound velocity which connects to the EOS.

The price one has to pay for a 'clock' consists in more complex shapes [8, 9, 10] due to the presence of spectators. In contrast, at energies beyond 10A GeV one can essentially start from 'simple' almond or elliptic shaped participant clusters of nucleons whose evolution generating dominantly in plane 'elliptic' flow was considered by Ollitrault [11] in the early nineties. However the spectator clock is no longer operative.

But even in this (nowadays 'low to intermediate') energy regime the present knowledge on the properties of compressed nuclear matter is not satisfactory.

Hopes that pion yields, measured in the mid-eighties, would be a textbook signal of a stiff EOS [12] have not materialized in the sequel. For possibly related reasons, the interpretation of pion isospin *ratio* data in helping to constrain the EOS of asymmetric systems is not settled [13, 14].

The use of positively charged kaons,  $K^+$ , in the subthreshold region proposed by [15] has been more successful. It is based on the principle that  $K^+$  are produced in larger amounts if the nuclear EOS is soft due to the higher achieved density causing more frequent collisions. This effect is enhanced in the deeply subthreshold energy regime because the production of  $K^+$  then requires multi-step reactions, including  $\Delta$  production, in the medium. In addition, the relatively low reabsorption cross sections are supposed to favor a good memory of the high density phase.

Using data from the KAOS Collaboration on heavy ion systems of varying size (namely C+C and Au+Au) and hence achieved density [16], two theoretical groups [17, 18] concluded that the so-called 'soft' EOS (see later) was best suited to explain the data. Despite this encouraging success some questions remain open. The kaon is very rare at the lowest measured incident energy, 0.8A GeV, where the sensitivity to the nuclear EOS is largest and one has to ensure that all 'bulk' observables (multiplicities, clusterization, stopping, flow) are under control. On the experimental side some desirable data, needed to complete the picture, are still missing: when switching from carbon to gold one is varying, besides the size, also the proton-neutron asymmetry, but the isospin partner,  $K^0$ , has not been measured at 0.8A GeV. Also, detailed experimental data on the nucleonic observables in C+C, needed to corroborate the simulated densities and momentum dependencies, are not

available.

Clearly other observables such as particle flow are welcome in order to confirm the conclusions from the 'kaon method'.

In a study [19] of Au+Au collisions covering the beam energy range of  $0.25A$  to  $1.15A$  GeV the EoS Collaboration made an attempt to establish a 'complete characterization of squeeze-out' (preferential emission out of the reaction plane) including a simultaneous consideration of 'three categories of collective motion' (radial and sideward flow and squeeze-out). From the work which was focused on the  $0.6A$  GeV data, the authors concluded at the time (1996) that 'the QMD (a transport code [20]) comparisons do not show a level of agreement with the data that justifies inferences about nuclear incompressibility'.

Almost 10 years later (2005) the FOPI Collaboration published [21] an excitation function of 'elliptic flow' (see later) extending from  $0.09A$  to  $1.5A$  GeV beam energy for  $Z = 1$  particles, also in the Au+Au system. The data were compared to the predictions from four different transport codes. The conclusion was 'no strong constraint on the EOS can be derived at this stage'.

A transport theoretical study of sideflow and elliptic flow data (restricted to emitted protons) both from the BEVALAC and the AGS accelerators was undertaken in [8]. The authors characterized their 'trial' EOS by the incompressibility  $K_0$  of symmetric nuclear matter around saturation density ( $\rho = \rho_0 \approx 0.16 \text{ fm}^{-3}$ ). An EOS labeled by  $K_0 = 167$  MeV was adjusted to the experimental data on directed flow at incident energies below  $1A$  GeV, with a better description of the higher energy data using  $K_0 = 200$  MeV. The elliptic flow data seemed to require  $K_0 = 300$  MeV.

In the present work we intend to improve the situation in the  $1A$  GeV regime. Profiting from extensive flow data published recently by the FOPI Collaboration [22] we take here specifically a close look at the elliptic flow data, taking advantage of the afore-mentioned clock. In doing so

1. we use not only protons, but also two- and three-nucleon clusters that are emitted in Au+Au collisions in the incident beam energy range from  $0.4A$  to  $1.5A$  GeV and that have larger flow signals than single nucleons
2. we use not only mid-rapidity data, but use the information from 80% of the target-projectile rapidity gap; as we will show this information can be lumped into a single observable.

The data are confronted to a well established transport code, Isospin Quantum Molecular Dynamics, IQMD [23, 24] using various phenomenological EOS to assess the EOS that is most compatible with the FOPI data. Four Skyrme type parameterizations are available in the code:  $H$  ('stiff'),  $S$  ('soft'),  $HM$  ('stiff momentum dependent'),  $SM$  ('soft momentum dependent'). As in [8] we characterize the EOS (for details see [24]) by saturation density incompressibilities:  $K_0 = 200$  ('soft') and  $K_0 = 380$  ('stiff').

We also estimate an error band from uncertainties in the data and compare to some recent representative microscopic EOS calculations.

In the following section we present the analysis of the elliptic flow data obtained by FOPI [22] and the resulting FOPI-IQMD constraint on the EOS. Dynamical details from the IQMD simulations are presented in section 3 and the constraints for the EOS obtained from the FOPI to IQMD comparisons are confronted with representative theoretical calculations in section 4. Finally, in section 5 we briefly discuss the obtained results and the needs for future efforts.

## 2. Analysis and results

A comprehensive documentation on flow data in the SIS energy range measured by the FOPI Collaboration is available in [22]. We shall therefore be brief here.

Owing to collective flow phenomena, discovered experimentally in 1984 [25, 26], it is possible to reconstruct the reaction plane event-by-event and hence to study azimuthal correlations relative to that plane. The well established parameterization [27, 28] of the observed azimuthal,  $\phi$ , distributions is used:

$$u = (\gamma, \vec{\beta}\gamma) ; \quad u_t = \beta_t\gamma \quad (1)$$

$$\frac{dN}{u_t du_t dy d\phi} = v_0 [1 + 2v_1 \cos(\phi) + 2v_2 \cos(2\phi)] \quad (2)$$

$$v_0 = v_0(y, u_t) ; \quad v_1 = v_1(y, u_t) ; \quad v_2 = v_2(y, u_t) \quad (3)$$

$$v_1 = \left\langle \frac{u_x}{u_t} \right\rangle = \langle \cos(\phi) \rangle ; \quad v_2 = \left\langle \left( \frac{u_x}{u_t} \right)^2 - \left( \frac{u_y}{u_t} \right)^2 \right\rangle = \langle \cos(2\phi) \rangle \quad (4)$$

Here we introduced the longitudinal (beam axis) rapidity  $y$  in the (*c.o.m.*) reference system and the transverse (spatial) component  $t$  of the four-velocity  $u$ , given by  $u_t = \beta_t\gamma$ . The 3-vector  $\vec{\beta}$  is the velocity in units of the light velocity and  $\gamma = 1/\sqrt{1 - \beta^2}$ . Throughout we use scaled units  $y_0 = y/y_p$  and  $u_{t0} = u_t/u_p$ , with  $u_p = \beta_p\gamma_p$ , the index  $p$  referring to the incident projectile in the *c.o.m.*. In these units the initial target-projectile rapidity gap always extends from  $y_0 = -1$  to  $y_0 = 1$ . In [22] the transverse momentum method [29] was used including all particles identified outside the mid-rapidity interval  $|y_0| < 0.3$  and excluding identified pions.

In Fig. 1 we show a sample of proton 'elliptic',  $-v_2$ , flow data from the FOPI Collaboration (black dots with error bars) together with simulations using IQMD with a stiff version of the EOS (HM, red) and a soft version (SM, blue), see Fig. 3 for details to which we shall come back later. The reaction is Au+Au at an incident energy of 1.2A GeV. In [22] many more such data spanning the incident beam energy range 0.15 – 1.5A GeV and varying centrality and system composition and size are shown.

By plotting  $-v_2$  (rather than  $+v_2$ ) one sees in this energy regime an enhancement of strength around mid-rapidity, i.e. predominantly out-of-plane emission, which was given the suggestive name 'squeeze-out' in pioneering, and predictive, theoretical work [30] on the subject. Nowadays this phenomenon is named elliptic flow avoiding to conclude on the importance of shadowing and density gradients. At these energies the elliptic flow changes sign at high  $|y_0|$  becoming predominantly in-plane.

As in earlier FOPI work, collision centrality selection was obtained by binning distributions of the ratio of total transverse to longitudinal kinetic energies in the center-of-mass system, *ERAT*. We estimate the impact parameter  $b$  from the measured differential cross sections for the *ERAT* using a geometrical sharp-cut approximation. We wish to stress here that we have used the same procedure (*ERAT*) for the simulations: the impact parameter, not accessible directly by experiment, does not enter the analysis of the theoretical events. A similar procedure was used to correct for finite resolution of the reaction plane orientation( see [22]).

We characterize the centrality by the interval of the scaled 'impact parameter'  $b_0$  defined by  $b_0 = b/b_{max}$ , taking  $b_{max} = 1.15(A_P^{1/3} + A_T^{1/3})$  fm. The centrality chosen for the figure

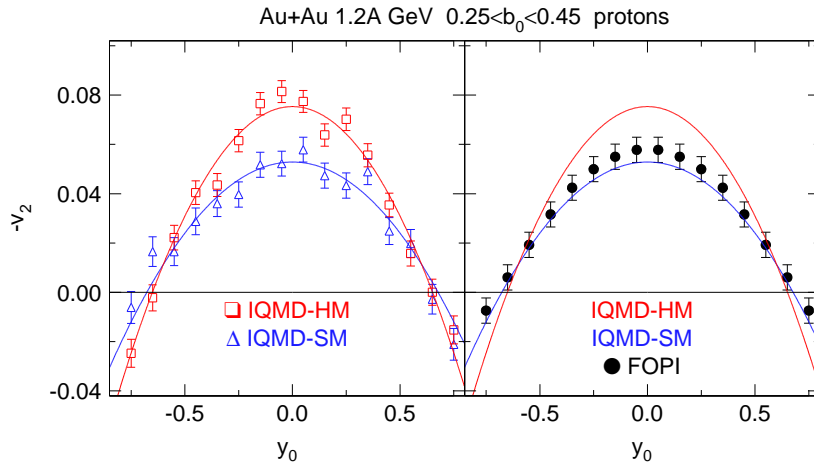


Figure 1: Proton elliptic flow data,  $-v_2(y_0)$ , and IQMD-SM/HM simulations. See text for further explanations.

is  $0.25 < b_0 < 0.45$ . The choice of an optimum centrality for this study was guided by the intention to compromise between the need for sufficiently sized 'shadow bars', composed by the spectator nucleons, on one side and the requirement of sufficient compression in the participant volume, a condition demanding a maximum size (maximum centrality) of the participant matter.

Taking a closer look at  $-v_2(y_0)$  we see that the predicted shape is sensitive to the EoS *in the full rapidity range*. To take advantage of this feature we introduce a quantity dubbed  $v_{2n}$  defined by  $v_{2n} = |v_{20}| + |v_{22}|$  where the parameters are fixed by a fit to the flow data using  $v_2(y_0) = v_{20} + v_{22} \cdot y_0^2$  in the scaled rapidity range  $|y_0| < 0.8$ . Such fits to the simulation data (here the error bars are of statistical origin) are shown in the left panel of Fig. 1 and then confronted with the experimental data (the error bars are now dominated by systematic errors) in the right panel. While  $v_{20}$  alone characterizes the flow at mid-rapidity only, and the algebraic addition  $v_{20} + v_{22}$  determines the flow at  $y_0 = 1$  the quantity  $v_{2n}$  combines features at both rapidities. The centrality is for  $0.25 < b_0 < 0.45$  and low momenta are cut off both in the data and the simulations. The cutting out of low transverse momenta, or equivalently, of scaled transverse 4-velocities ( $u_{t0} < 0.4$ ), originally forced by apparatus limitations, actually turns out to raise the sensitivity of  $v_2$  to the EOS as flow is generally converging to zero at low momenta (see e.g. [22]).

The  $v_{2n}$  obtained for Au+Au between  $0.4A$  and  $1.5A$  GeV are shown in Fig. 2 for protons (lower left) and deuterons (lower right), tritons (upper left) and  $^3\text{He}$ . As the beam energy dependencies are rather weak, we indicate the average behavior by straight lines. The comparison of the data for  $v_{2n}$  with the calculations shows a rather convincing preference for SM. The sensitivity is large: there is a factor  $1.63 \pm 0.06$  between HM and SM, a difference exceeding significantly the indicated experimental error bars. If we compare this factor with the fluctuations of the experimental data points around the average values (dashed lines) we can estimate the uncertainty of the deduced EOS.

To obtain quantitative conclusions on the EOS characterizer  $K_0$  for the energy range investigated in the present work we have constructed Table I which contains the relevant numbers (read off from the figure) with error bars.

The Table lists the average (straight lines in the figure)  $v_{2n}$  obtained, in order, for

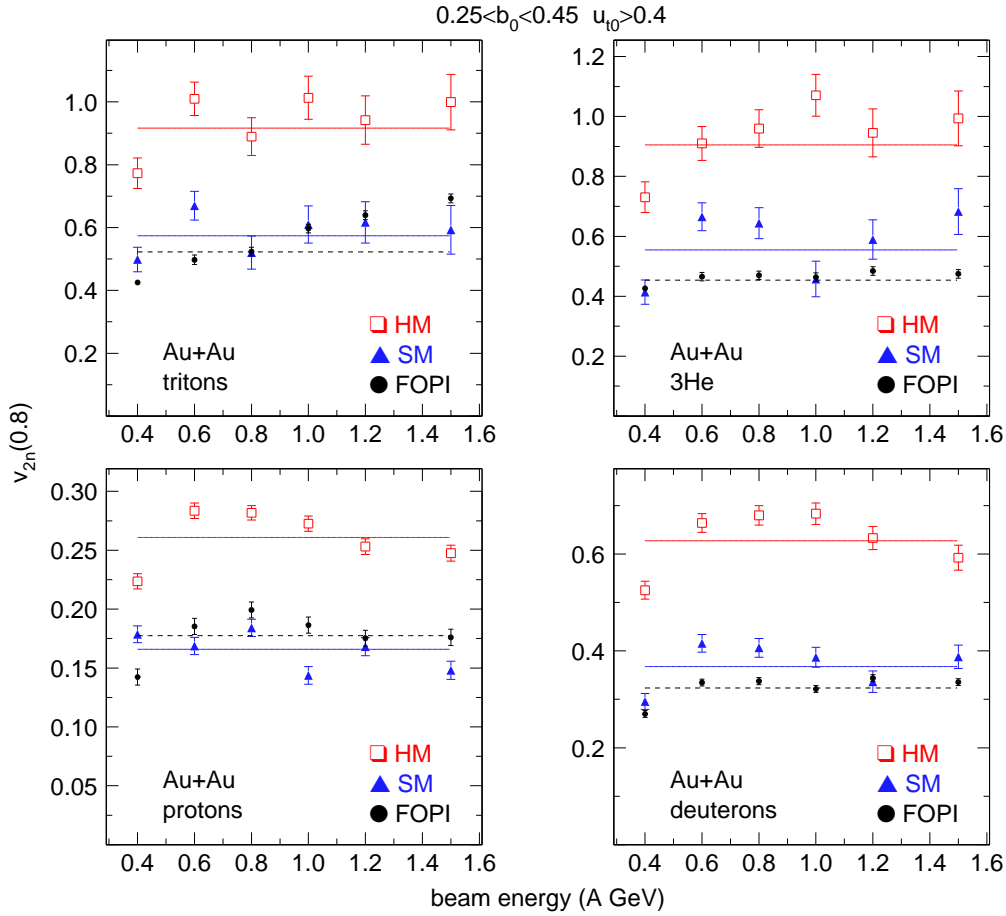


Figure 2: Elliptic flow  $v_{2n}$  for protons, deuterons, tritons,  $^3\text{He}$  as function of incident beam energy.

SM, HM and FOPI, the ratio between HM and SM, the difference between HM and SM, the difference between FOPI and SM, and in the last column the modification of  $K$  (for SM) needed to account for the difference FOPI-SM, assuming for simplicity a linear interpolation between the  $K_0$  for HM and SM. From the information using four different particles we thus obtain a weighted average  $K_0 = 190 \pm 30$ , while the theoretical ratio between HM and SM is  $1.63 \pm 0.06$ . The used procedure is somewhat naive, but this is deemed uncritical considering the adopted error on  $K_0$ .

We have plotted in Fig. 3 the resulting EOS with its uncertainty band. For comparison we have also plotted the 'trial' EOS, HM and SM, used in the simulations. For the valid density range, indicated by vertical bars, see Section 3. Note the phenomenological EOS HM and SM include the saturation point at  $\rho/\rho_0 = 1$ ,  $E/A = -16$  MeV by construction. This fixes the absolute position of the curves: the heavy ion data are only sensitive to the shape, i.e. the pressure which is essentially the derivative. Therefore the uncertainty of this fundamental point, about 0.5 MeV for the binding energy and 0.1 fm for  $\rho_0$ , is *not* included in the uncertainty band. This will be important later when comparing to some representative theoretical EOS, section 4. However, we can already at this stage conclude, in complete agreement with ref. [8] that a stiff EOS, characterized by  $K_0 = 380$  MeV is not in agreement with flow data in the incident energy range  $(0.4 - 1.5)A$  GeV. For  $0.4A$  GeV this had also been suggested in [31].

Table 1: Derivation of the effective  $K$  using the elliptic flow observable  $v_{2n}$

	$v_{2n}$ SM	$v_{2n}$ HM	$v_{2n}$ FOPI	HM/SM	HM-SM	FOPI-SM	$\Delta K$ MeV
$^1\text{H}$	$0.1658 \pm 0.0030$	$0.2609 \pm 0.0027$	$0.1774 \pm 0.0028$	$1.57 \pm 0.07$	0.0951	+0.0116	$+22 \pm 8$
$^2\text{H}$	$0.3676 \pm 0.0080$	$0.6274 \pm 0.0087$	$0.3237 \pm 0.0029$	$1.71 \pm 0.08$	0.2598	-0.0439	$-30 \pm 8$
$^3\text{H}$	$0.5740 \pm 0.0214$	$0.9161 \pm 0.0252$	$0.5223 \pm 0.0048$	$1.60 \pm 0.08$	0.3421	-0.0517	$-27 \pm 17$
$^3\text{He}$	$0.5540 \pm 0.0217$	$0.9048 \pm 0.0265$	$0.4537 \pm 0.0050$	$1.63 \pm 0.16$	0.3501	-0.1010	$-52 \pm 18$

### 3. Simulations: the scenario

In order to determine the EOS empirically, it is reasonable to start from low densities/pressures/temperatures and gradually raise these characteristics using sufficiently close steps. This is necessary to become aware of discontinuities (even modest ones) possibly indicating important structural changes.

The first step is to constrain the relevant density range. Isoscalar giant monopole resonance (GMR) data ('breathing modes') have been used [32] with the claim to determine the incompressibility around saturation density ( $\rho = \rho_0 = 0.16 \text{ fm}^{-3}$ ) where, by definition, the pressure in infinite symmetric nuclear matter is zero. An incompressibility  $K(\rho_0) = K_0$  of  $210 \pm 30 \text{ MeV}$  was deduced in [32] from the monopole energies.

In this context, it is interesting that recently some new insights have come up concerning the  $K_0$  value. In [33] the authors have pointed out that the GMR actually tests compressibility at about  $2/3\rho_0$  which is the *average* density of large nuclei whose finite depth surface area is not negligible. The 'microscopic' theories using energy density functionals (EDF), adjusted to reproduce the GMR data, then actually have to extrapolate to  $\rho_0$  leading according to [33] to  $K_0 = 230 \pm 40 \text{ MeV}$ , the error reflecting fluctuations between different EDF.

One should not expect that the value for the incompressibility of nuclear matter is directly comparable to the one used to characterize the tentative EOS adjusted to reproduce heavy ion flows with transport codes, since the latter, as we will show, refer to data associated to densities significantly larger than  $\rho_0$ , and there is no basic principle which requires that the EOS is of simple parabolic shape over large ranges of density.

Whereas the determination of the nuclear matter EOS with GMR data is an approach to saturation density 'from below', our extensive IQMD simulations of the observations discussed in the present work suggest that in the FOPI experiments, we are advancing towards saturation density 'from above'.

In contrast to model calculations done in an effort to reproduce the data, the simulations discussed in this section are done at a single impact parameter, since our goal is to elucidate the reaction scenario and to characterize which 'typical' densities are probed with the proton elliptic flow that has been extracted from the FOPI experiments. For this purpose one has to determine at which times – in the course of the collision – and medium conditions are linked with and influence the most the development of the elliptic flow. Here, we restrict ourselves to the study of the  $^{197}\text{Au}+^{197}\text{Au}$  system at an 'intermediate' impact parameter  $b = 3fm$ . It is close to the upper limit of the centrality range chosen for the experimental data in Figs. 1 and 2.

In Fig. 4 various quantities are plotted as a function of time scaled to the passing time

## HM/SM/FOPI

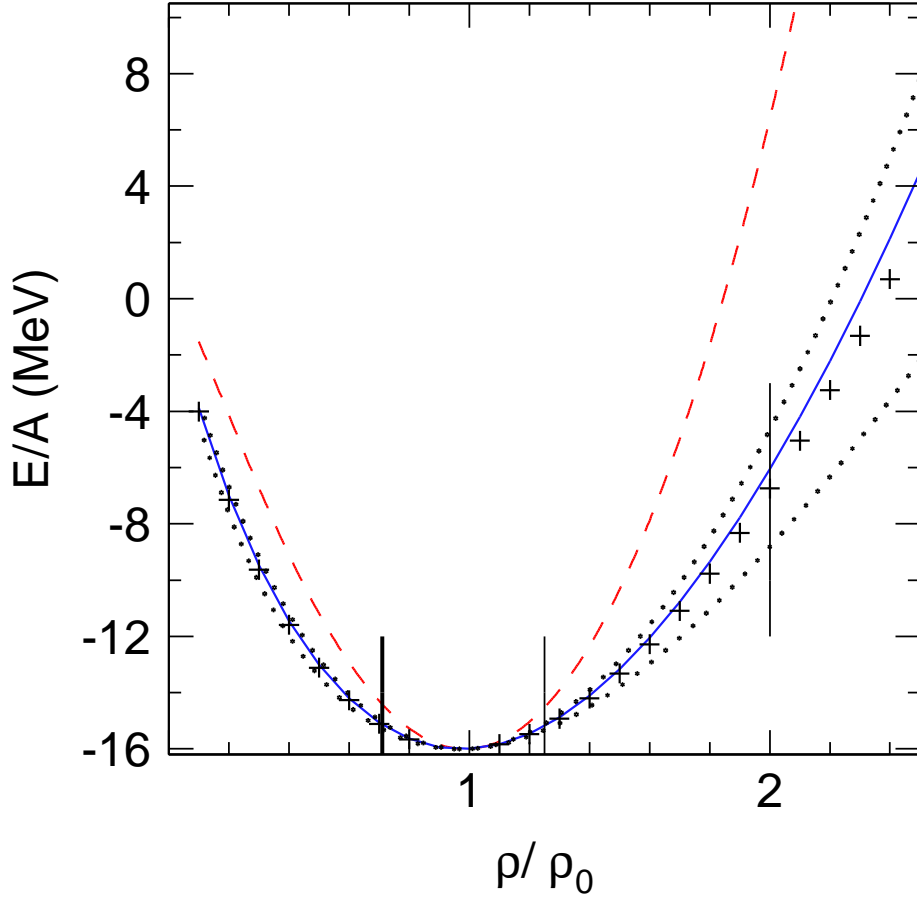


Figure 3: Various symmetric nuclear matter EOS. Dashed (red) HM, full (blue) curve, SM. The dotted curves and the thin vertical bars delimit the FOPI EOS (crosses) constraints. The thick vertical bar is the density relevant for the GMR according to [33].

$t/t_{pass}$ , the time the nuclei pass each other is approximated by  $t_{pass} = 2R/u_p$ , where  $u_p$  was introduced in section 2. The time zero is defined as the the moment projectile and target nucleons have the *first hard collision*. Typical values of  $t_{pass}$  for various incident energies are listed in Table 2. The top panel of Fig. 4 shows on the left hand side the normalized density,  $\rho/\rho_0$  (where  $\rho_0$  is the nuclear matter ground state density) seen by the protons in the central region of the collision. The central region is defined as a sphere with a radius of 1 fm around the center. This data is shown for reference and indicates the maximum density reached in those reactions. For a soft EOS higher densities are reached than for a hard EOS because the acting potential is less repulsive. The upper right panel depicts the mean density seen by all protons with transverse 4-velocities  $u_{t0} > 0.4$  and  $|y_0| < 0.8$  in the final stage of the reaction. This cut was adopted in the analysis of the FOPI data and we note that this selection removes most of the spectator particles. One observes that the maximum of density probed by these protons in the course of the collision is reached at around the full overlap of the incoming system ( $t/t_{pass} = 0.5$ ), and that the 'soft' EOS takes a slightly longer time to reach the maximum density, and reaches higher

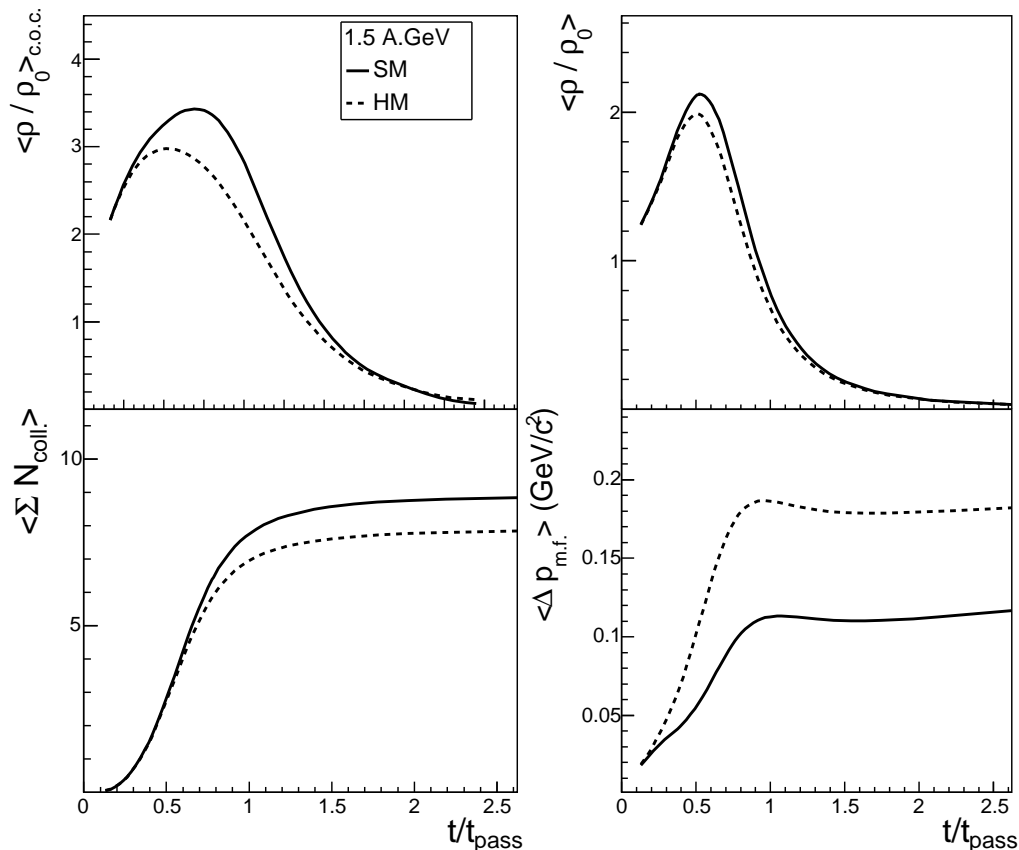


Figure 4: IQMD predictions of the time evolution of various quantities in Au+Au collisions at 1.5A GeV incident energy and an impact parameter  $b = 3 \text{ fm}$  for various parameterizations of the EOS: soft EOS (SM) and hard EOS (HM), distinguishable through different line styles. The various quantities from left top to right bottom panels are: the reduced density probed by protons in the center of the colliding system, *idem* for all protons finally in the phase space region defined by  $|y_0| < 0.8$  and  $u_{t0} > 0.4$ , the integrated (since time zero) sum of collisions experienced by these protons and their integrated momentum change due to the mean field (force).

densities, as regard to the 'hard' EOS. The mean time-integrated number of collisions for selected protons is shown in the lower left panel, and in the right panel their mean integrated momentum transfer caused by the potential. Obviously nearly all collisions have taken place until the passing time and most of the momentum transfer due to the potential has been achieved, i.e. the influence of the potential becomes very small because the system is getting diluted. We only see a slight dependence on the stiffness of the EOS in the number of collisions, caused by the different mean free paths of nucleons due to the different densities reached. However, the momentum transfer caused by the potential in the 'hard' case is much larger than in the 'soft' one, which reflects of the higher repulsion of the hard equation of state. Similar conclusions can be drawn for all incident energies that we have simulated (0.15 to 1.5 A.GeV). A summary of the maximum densities reached during the time evolution of the reaction for a range of beam energies is shown in Fig. 8.

Fig. 5 synthesizes the dependence of the variable  $v_{2n}$  as a function of reduced time  $t/t_{\text{pass}}$ . This observable saturates only after two to three times the passing time with identical dependence for soft and hard EOS. To underline the similarity we applied a

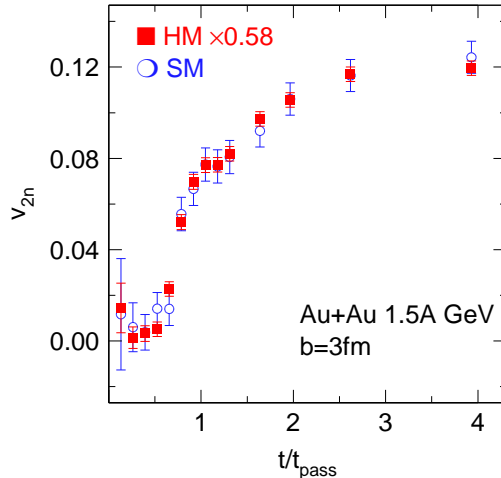


Figure 5: IQMD results for  $v_{2n}$  (see Section 2) as a function of scaled time  $t/t_{pass}$  for different EOS. The values of  $v_{2n}$  calculated with a hard EOS have been multiplied by a factor of 0.58 (filled squares) to show the similarity with the shape of the SM predictions (open circles). One observes that the ratio of  $v_{2n}$  versus time reflects closely the ratio of the integrated momentum changes due to the mean field gradients shown in Fig.4.

Table 2: Passing time (see text) of the projectile and the target as a function of the incident energy in the  $^{197}\text{Au} + ^{197}\text{Au}$  collisions

$E_{inc.}$ (A.MeV)	150	250	400	600	800	1000	1200	1500
$t_{pass}$ (fm/c)	48.3	37.4	29.6	24.1	20.9	18.7	17.1	15.3

scaling factor of 0.58 to the data for the hard EOS in Fig. 5. Despite the fact that the absolute size of the signal differs by almost a factor of 2 for the EOS under considerations, this difference becomes stable fairly quickly in the course of the reaction. The elliptic flow signals  $v_n$  themselves need rather long times to obtain their final (observed) shape. This is illustrated in more detail in Fig. 6: the value of  $v_2$  at mid-rapidity stabilizes quite fast, already at the full passing time, but it needs nearly twice as long to reach its final shape close to the target and projectile rapidities.

We demonstrated that the mid-rapidity signal of  $v_2(y_0)$  develops rather rapidly within the IQMD model, stabilizing already after the passing time. This is an indicator that the spectator clock is working as anticipated. The elliptic flow at target and projectile rapidities takes a longer time to evolve since it originates also from late interactions with the spectator material.

A decomposition of the elliptic flow into potential and collisional contributions will elucidate the underlying reaction mechanisms. In Fig. 7 it is illustrated how the final  $v_2(y_0)$  is obtained by NN collisions only, the mean field only, and by both operating together. The IQMD model allows to record the moment change due to collisions and due to potential separately for each time step. Integrating all contributions over the reaction time will yield the total momentum transfer vector due to the potential and analogously caused by the collisions. Both quantities have been analyzed to obtain  $v_2(y_0)$ . Note, that

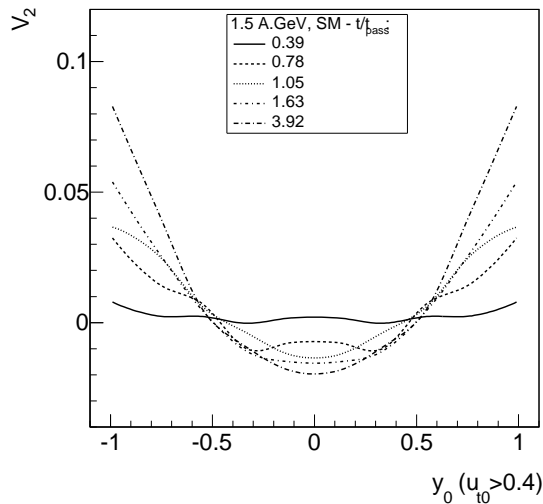


Figure 6: Results of IQMD calculations for the elliptic flow  $v_2$  of protons as a function of scaled rapidity  $y_0$  at various values of the scaled time  $t/t_{pass}$  (different line styles) and for an incident energy  $E_{beam} = 1.5$  A.GeV. The protons are selected to have high transverse momenta  $u_{t0} > 0.4$  (see Section 2). The IQMD calculations are the same as in Fig. 4 for a SM EOS.

the values of those different  $v_2(y_0)$  contributions cannot be simply added, since they do not reflect an absolute magnitude and the final momentum is obtained by a vector sum of the different contributions.

We find the following features:

a) The collisional contribution to  $v_2$  alone is small and little affected by different EOS. This suggests that moderate medium changes of the NN cross sections that go beyond 'zero order' Pauli blocking corrections would not critically affect our conclusions on the EOS. Furthermore, the collisions by themselves cannot predict the measured elliptic flow. This illustrates the inadequacy of the cascade approaches for flow observables at these beam energies.

b) The elliptic flow signal  $v_2$  is more affected by the potential effects. One observes significant differences of the  $v_2(y_0)$  when applying different equations of states.

Following this observation - that the elliptic flow signal is dominated by the acting potentials - we propose to construct a characteristic density which is connected to the elliptic flow of protons by calculating the mean value of the density seen by all protons with a final  $u_{t0} > 0.4$  *weighted by the strength of the force due to the local mean field*. This quantity integrated up to the full passing time is displayed by the line in the right hand-side of Fig. 8 as a function of bombarding energy. This variable is shown for the SM EOS which has been qualified by the FOPI measurements. The shaded area represents the variances of the "force-weighted" densities (*corresponding to finite size effects*). Using such a method we are not limiting ourselves to some small most central volume of the system a procedure which then naturally yields significantly larger densities. Those are depicted in the left hand-side of Fig. 8. The maximum density in the central volume  $max < \rho/\rho_0 > (t)$  is shown as function of bombarding energy, as well as the maximum density seen by all protons with final  $|y_0| < 0.8$  and the maximum density of protons with  $|y_0| < 0.8$  and  $u_{t0} > 0.4$ . In the innermost center of the collision densities up to  $3.5\rho_0$  are reached at the highest beam energies measured by the FOPI collaboration. The density experienced by all protons measured in the region around mid-rapidity  $|y_0| < 0.8$  is substantially lower

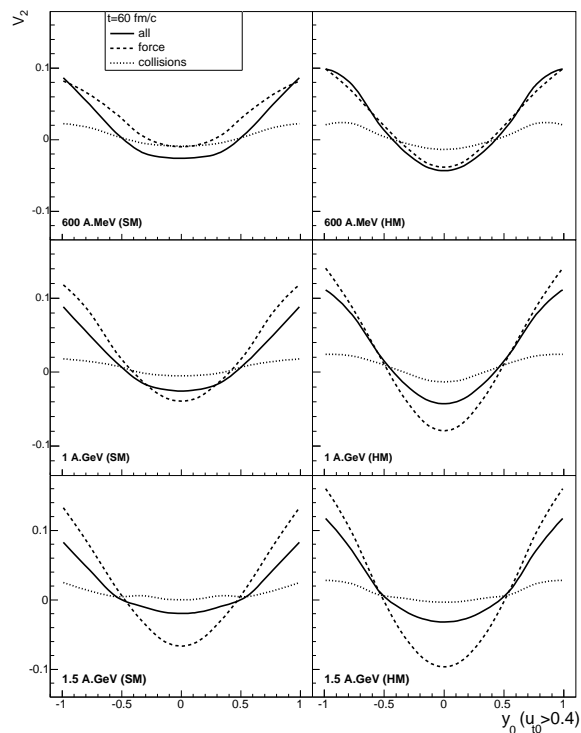


Figure 7: Elliptic flow  $v_2$  of protons having finally a high transverse momentum  $u_{t0} > 0.4$  (see Section 2) as a function of their scaled rapidity  $y_0$  predicted by IQMD. Results for SM and HM EOS's are shown at 0.6, 1 and 1.5A GeV incident energies at the late time  $t = 60$  fm/c independent of energy. The total elliptic flow ('all', black lines) is presented along with its decomposition into the two contributions, i.e. mean field ('force', dashed lines) and collisions (dotted lines).

(up to  $2\rho_0$ ), and this value is not changed by the additional experimental cut  $u_{t0} > 0.4$ .

Our method of averaging with the strength of the force is in the same spirit as proposed in [33] for the GMR. As can be seen in Fig. 8, the gap to the  $2/3\rho_0$  data of the GMR could be closed by lowering the incident energies at least down to 0.1 A.GeV. Even if the densities extracted here are smaller than the maximum density reached during the collisions, the presence of the highly compressed matter (up to  $3\rho_0$ ) is mandatory for building up the high density gradients leading to the repulsion of particles and finally the elliptic flow signals.

#### 4. Comparison to microscopic calculations

In view of the large number of proposed nuclear matter EOS in the literature, see for example the recent discussion of EOS derived using 240 (!) 'phenomenological' (Skyrme interactions) approaches in [34], we cannot here compare our constrained 'experimental' EOS in Fig. 3 with all these various predicted behaviors, but hope that future theoretical efforts will consider our results for the density range up to  $\rho/\rho_0 = 2.5$ .

By 'microscopic' calculations we define here theoretical efforts to calculate the infinite nuclear matter EOS using nucleon-nucleon and pion-nucleon scattering data and some information on multi-body forces (3N, 4N) from light nuclear clusters, including of course the deuteron, *without introducing further ad hoc parameters*. Taranto et al. [35] have recently tested five such models for their consistency with known astrophysics and nuclear

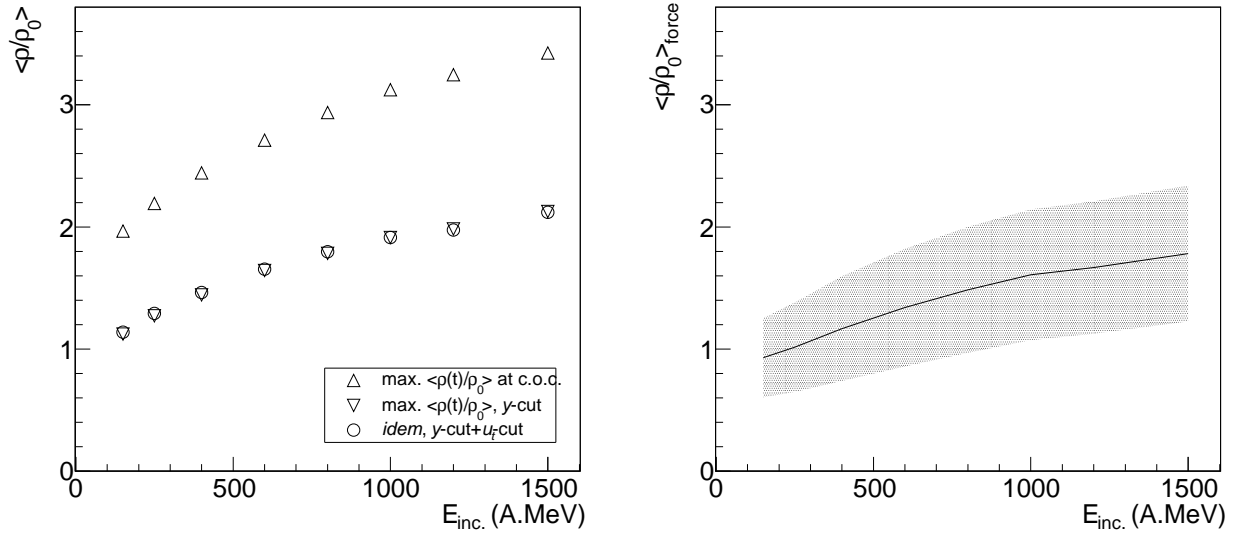


Figure 8: Left side: The maximum of the density  $\langle \rho(t)/\rho_0 \rangle_{max}$  reached in the central volume of the collision (shown in Fig. 4 for 1.5A GeV) as a function of beam energy is shown as open triangles, the maximum of the density  $\langle \rho(t)/\rho_0 \rangle_{y-cut}$  for protons finally in the rapidity range  $|y_0| < 0.8$  as reversed triangles and as open circles the maximum of  $\langle \rho(t)/\rho_0 \rangle_{y-cut+u_t-cut}$  seen by protons with  $|y_0| < 0.8$  and  $u_{t0} > 0.4$ . Right side: "Force-weighted" mean value of the reduced density (see text) seen by protons  $u_{t0} > 0.4$  and  $|y_0| < 0.8$  in their final configuration averaged until the passing time. The error bars represent the standard deviations of the distributions.

physics constraints. They came up with open questions concerning the predictions for high densities ( $\rho > 3\rho_0$ ) that one needs to know in compact star modeling. An intriguing point was that three of the models violated causality at the predicted central densities and the suggestion that even Dirac-Brueckner-Hartree-Fock (DBHF) calculations may be in error due to approximations made in order to make the calculation tractable.

We choose here to confront three *representative* microscopic calculations with our new constraints. First a DBHF calculation [36] of both symmetric and pure neutron matter which was presented in a conveniently parameterized form allowing to estimate with use of the parabolic assumption (involving  $\delta^2$ ) the deviation of the EOS in going from strictly symmetric to Au-like ( $\delta^2 = 0.0391$ ) composition, where  $\delta = (N - Z)/(N + Z)$ . The second comparison uses work from the 'Idaho group' [37] allowing to compare the historically earlier DBHF approach with the more recent chirally motivated theories. Finally, we compare with two different EOS published in 2005 [38] one having the interesting feature of including the possibility of (virtual)  $\Delta$  excitations *explicitly*.

The EOS calculated with DBHF in [36] using the Bonn A [39] nucleon-nucleon potential (full green curve) is confronted in Fig. 9 with our constrained FOPI-IQMD EOS (shaded band around the median black curve). The authors [36] have made efforts to check the validity of averaging approximations often used in DBHF to reduce the computational cost.

As mentioned before we have also estimated the 'correction' to the symmetric EOS due to the degree of isospin asymmetry in gold (Au), see the dashed curve. It is located roughly 1 – 1.5A MeV above the symmetric system. It is visible that the shape of the 'Au' EOS is not dramatically different from the strictly symmetric matter EOS. Of course the heavy ion flow data, being sensitive only to the pressure, i.e. essentially the derivative of such curves,

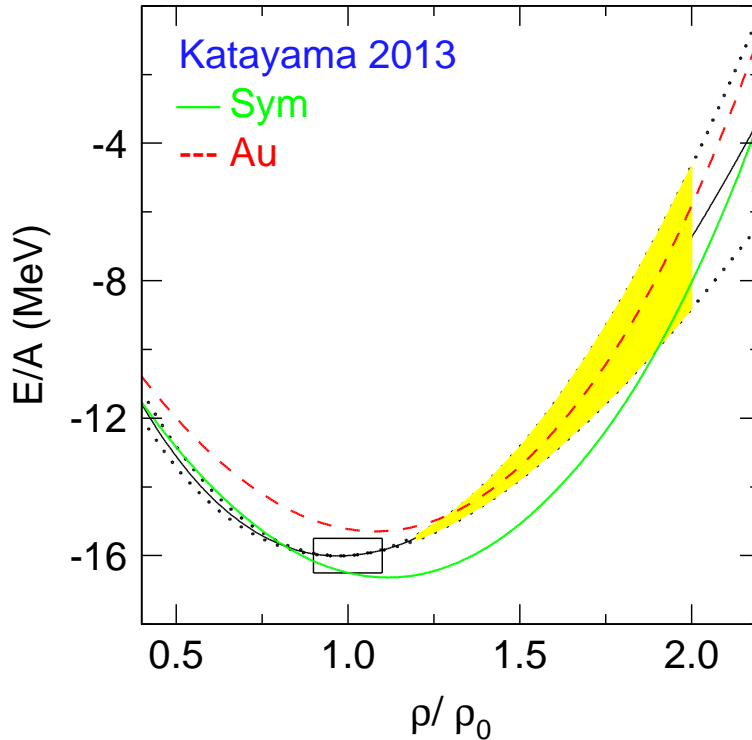


Figure 9: Symmetric nuclear matter EOS from ref. [36] using Bonn A potential (full green curve). The dashed red curve is the EOS for Au-like systems using neutron matter calculations from [36]. The shaded error band surrounding the black curve is the FOPI-IQMD constraint.

does not allow to determine the absolute vertical position of the energy/nucleon EOS. The uncertainty of this position is roughly indicated by the rectangle in the figure. As there seems no clear consensus on the widths of this 'saturation rectangle' in the literature we have adopted here approximately the sizes given in two theoretical papers, [40, 41] If one adopts conclusions from given observables (such as nuclear masses and electron-scattering data) one can come to tighter, but still model dependent limits. As just one example, one obtains very tight limits ( $<0.2$  MeV) on the bulk binding energy if one interprets the mass-number proportional coefficient as holding for infinite NM, see a recent effort in [42].

The narrowing 'error' band of the empirical curve in approaching the saturation point is a consequence of constraining the curve to cross the most probable saturation value and ignores the shown uncertainty of this very fundamental point.

Constraining the stiffness of pure neutron matter at densities significantly exceeding the saturation density is and will be a difficult task as realistic heavy ion systems, even at radioactive beam facilities, will not exceed  $\delta^2$  values larger than 5%. It is therefore not surprising that information relevant to compact star physics [43] is so far primarily limited to subsaturation densities that are accessible by other means.

In Fig. 10 we show two symmetric nuclear matter EOS from ref. [37]. One, full triangles, labeled 'DBHF' in the figure, is using a meson theoretic potential together with the DBHF method, the other, open triangles, labeled 'Chiral', makes use of effective field theory (EFT) with density dependent interactions derived from leading order chiral three-nucleon forces.

One can see that the DBHF curve tends to become stiffer at densities exceeding  $\rho >$

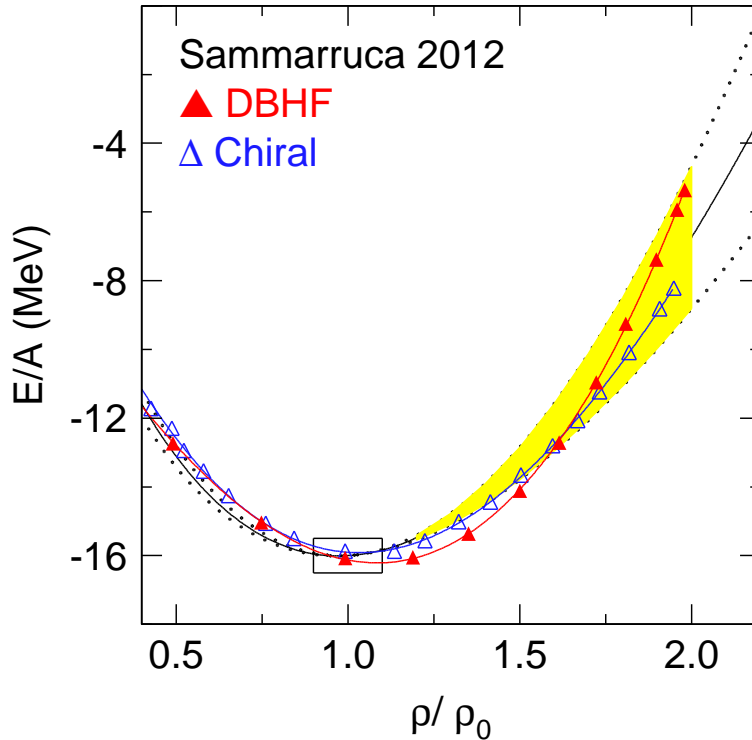


Figure 10: Symmetric nuclear matter EOS after ref. [37]. Full (red) triangles: DBHF calculation, open (blue) triangles: chiral effective field theory. The shaded band is the FOPI-IQMD constraint.

$1.5\rho_0$ . On the other hand the 'chiral' version seems to match close to perfectly with the FOPI-IQMD constraint (shaded). As the EFT approach, respecting QCD symmetries, is a low-momentum theory sorting the contributions of various order according to powers of momentum the question arises up to what density one can trust the predictions. In [44] Machleidt pointed out that chiral NN potentials do not make any reasonable predictions beyond 300 MeV laboratory energy. He ends up concluding that 'one may trust the chiral perturbation theory up to densities around  $4\rho_0$ '.

The treatment of the short range parts of the nucleon-nucleon forces outside of QCD lattice theory is still subject to different approaches, not only between the above mentioned DBHF and Chiral EOS, but also in some other 'chiral approaches to nuclear matter' [38]. As we wish to limit the scope and size of the present contribution, we will not describe or comment these various approaches. However we can show, see Fig. 11, how the theoretical investigations may use the FOPI-IQMD constraint as rough guide line.

Using the chiral approach, the authors [38] predict two rather different EOS depending on whether they include or not virtual  $\Delta$  excitations. See the figure caption. The predictions including the  $\Delta$  are in agreement with the empirical saturation point. The theory is not completely free of some adjustments that go beyond the use of  $\pi N$  and  $NN$  scattering data. The short-range parameters of the theory have been 'fine-tuned' to reproduce the ( $-16$ ) MeV binding energy per nucleon at saturation. However, the virtual  $\Delta$ -excitations then help to locate the EOS at the right horizontal place around  $\rho = 0.16 \text{ fm}^{-3}$ . A look at Fig. 11 shows that the  $\Delta$  leads to a rather marked stiffening of the EOS ( $K_0 = 304 \text{ MeV}$ ) projecting the curve outside the shaded FOPI-IQMD constraint. It is not obvious to us what this discrepancy means. It could be that the apparent 'heavy-ion EOS' actually

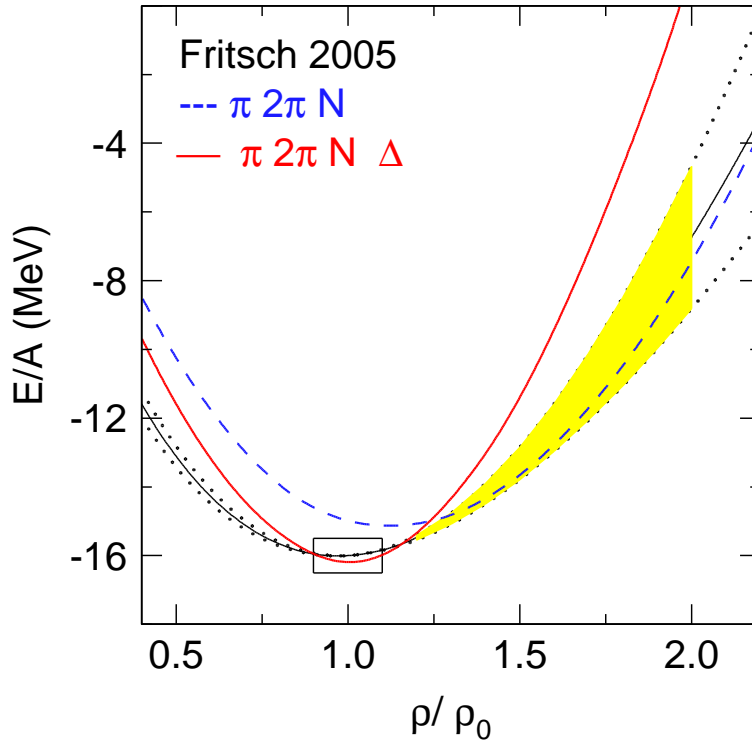


Figure 11: Symmetric nuclear matter EOS after ref. [38]. The dashed (blue) EOS curve includes pions and nucleons as active degrees of freedom. The full (red) curve includes effects from  $2\pi$  exchange with virtual  $\Delta$ -excitation. The shaded band is the FOPI-IQMD constraint.

differs from a 'cold' EOS because, due to the finite temperature in the reaction the  $\Delta$  are real rather than virtual. The theoretical ' $\Delta$  stiffness' could then be a dispersion effect rapidly changing with temperature. If so, it would be eminently important to pursue this question. Naively, one would expect that the (real) possibility to store energy internally into the nucleon (at high T) would lower the kinetic energies and hence the pressure and stiffness, some kind of mild 'phase transition' when new degrees of freedom open.

## 5. Discussion

We have shown in section 2 that a single parameter which we dubbed  $v_{2n}$ , characterizing elliptic flow over a large rapidity interval (80% of the initial gap) allows to discriminate rather clearly between a soft (SM) and a stiff (HM) EOS.  $v_{2n}$  differs by a factor 1.63 over an energy range extending from  $0.4A$  GeV to  $1.5A$  GeV when using IQMD, while the experiment allows to constrain  $v_{2n}$  within roughly a factor 1.1. The relevant density range was estimated from the simulations to span  $\rho_{max} = (1.1 - 3.0)\rho_0$ , where the high densities reached during the collisions are important for the evolution of the final elliptic flow pattern. This makes the 'flow method' competitive and complementary with the 'kaon method': the latter reaches such a high SM/HM discrimination only around  $0.8A$  GeV far below threshold. It is gratifying that both methods lead to the same conclusion, however.

In Fig. 12 the range of pressure and density assessed in this work is shown by the area enclosed by the dashed lines. The pressure for symmetric matter at zero temperature predicted by the FOPI-IQMD constrained EOS with  $\kappa = 190 \pm 30 \text{ MeV}$  is shown as magenta line. To put these results in context with others they are compared to the

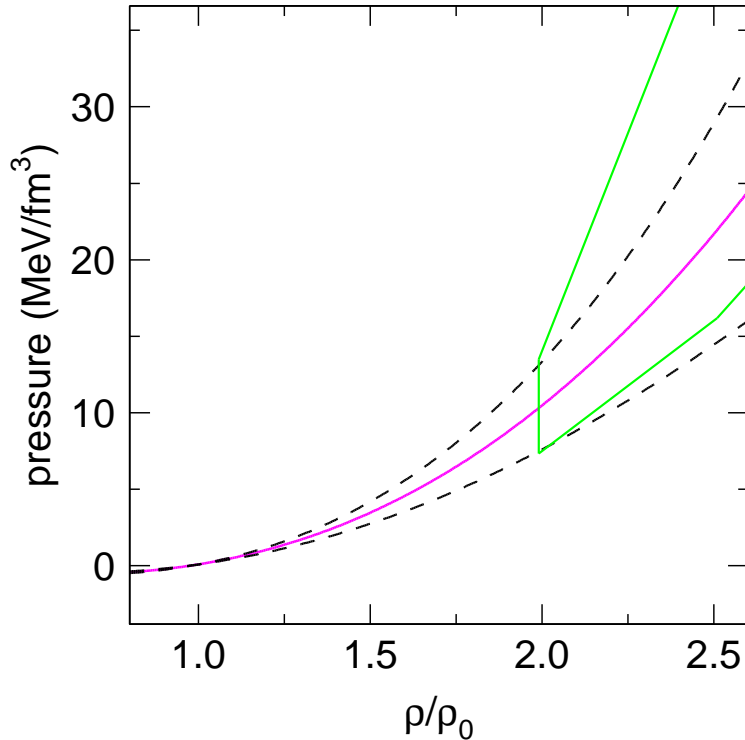


Figure 12: Nuclear EOS in terms of pressure versus density. The pressure as deduced from the soft EOS which was used in the IQMD model calculations is shown by the magenta line. The dashed curves enclose the error band in the determination of the relevant pressure region. The area framed with lines originates from the analysis of [8]

constraints reported in the analysis of [8] at higher energies and respective densities. Our data is in agreement with the earlier findings giving slightly more restrictive constraints towards a more soft nuclear matter EOS at higher densities.

Convincing conclusions on basic nuclear properties require a successful simulation of the full set of experimental observables with the same code using the same physical and technical parameters. For a number of observables this goal has been reached, for some other data this is not yet the case.

It is well known that in the beam axis system elliptic flow is not independent of the flow axis and hence the magnitude of the directed flow. In contrast to ref. [8], the IQMD model reproduces the directed flow using the same EOS parameters. In ref. [22] this is shown (Fig. 49) for directed flow of deuterons in the same beam energy and centrality range. Here too the experimental errors were significantly smaller than the HM/SM difference.

Furthermore, in the same work, Fig. 51, radial flow of the light clusters was well reproduced (and found to be insensitive to EOS).

Stopping information [47, 48] and Fig. 52 in [22] relevant to the question of in-medium nucleon-nucleon cross sections, requires still some fine tuning on the 20% level. Incomplete stopping could mockup a soft EOS if it is incorrectly accounted for in the simulations [45].

Pion yields, measured with 10% accuracy, [46], differ only by about 10% between the HM and SM options, and the yields were found to have about 20% lower values than the SM option of IQMD. It should be kept in mind that the elementary pion cross sections are known with limited precision.

Some less desirable features of our version of IQMD will not be hidden:

a) the momentum dependencies of protonic  $v_1$  are not correctly reproduced, while it is increasingly correct the heavier the cluster; this could be due to a lack of quantum fluctuations in a semiclassical code; we expect that fluctuations have a diminished influence on  $v_{2n}$  because it is determined by a large part of phase space;

b) the degree of clusterization is underestimated; this deserves further investigations.

It is worthwhile mentioning that in [22] some comparisons were also done with lower energy data. At  $0.15A$  GeV the difference HM/SM was found to be rather small. The deuteron elliptic flow was well reproduced by IQMD, Fig. 38. The small sensitivity to EOS at beam energies well below  $0.4A$  GeV is not surprising in view of the flatness of the energy/nucleon EOS (see Fig. 3) in this regime, implying relatively low pressures. We also remark that at  $0.25A$  GeV the  $v_1$  flow of all light clusters was well reproduced. The reproduction of low energy data, where the effect of the EOS is still moderate, is useful to ensure the adequacy of some technical parameters of the code.

Last, but not least, essentially the same IQMD code (except for some kaon specific sections) was used for the 'kaon method'.

Despite these encouraging results, there are two important points to be aware of:

1. data that are claimed to constrain such fundamental properties as is the EOS of nuclear matter require confirmation by independent experimental efforts
2. there is an urgent need to prove that the conclusions using a particular transport code, here IQMD, are not limited to using this particular code.

We shall briefly comment on these two points.

Before the 'experimental' EOS is finally ready for textbooks one needs a general consensus on the measured data with use of various apparatus. At the time of writing this goal is not yet reached in a satisfactory way. In ref. [8] two of the at that time available experimental data points on elliptic flow within the SIS/BEVALAC energy range (below  $2A$  GeV) survived the critical eye of the authors: a point ( $|v_2| \approx 7.7\%$ ) around  $0.4A$  GeV from the Plastic Ball Collaboration [49] and a point near  $1.1A$  GeV (6.2%) from the EOS Collaboration both obtained at the BEVALAC accelerator in Berkeley (USA) with a different apparatus. We could not find the (non-rotated) Plastic Ball value in the literature as the authors of refs. [49, 50] choose at the time the so called 'flow axis' as reference to determine elliptic flow. To our knowledge the AGS data [51] were not 'rotated' (see [22] for a brief discussion of the issue of rotated reference systems). A close comparison in [22] with the Plastic Ball's rotated data suggested disagreement with the FOPI data in at least part of the overlapping incident energy range. The  $1.1A$  GeV point accepted in [8] was first cited in [51], but we could not find a detailed documentation in the refereed literature on how possible apparatus cuts and other effects were taken into account. Optimistically, the  $1.1A$  GeV value is compatible with the FOPI data if one assumes a compensation of cut effects (present in the FOPI data) and slightly different beam energies.

In [22] comparisons to proton data from KAOS [52] used by Danielewicz [53] to tune momentum dependencies were also done. The agreement was acceptable but not perfect, see [22] Fig. 35 for details.

The second important point to be discussed is that the conclusions drawn from the comparison with simulation data obtained from various transport codes must be consistent. There are several issues that need further efforts by the community: momentum dependencies (including clean Lorentz covariance at beam energies exceeding  $1A$  GeV), clusterization and entropy balances, in-medium nucleon-nucleon reactions etc. Efforts to

bring transport code experts together, to see if a convergence of analyses results can be reached, have been done [54] but urgently need to be continued including energies up to FAIR accelerator design.

What can we say about the future besides asking for efforts to reach consensus on both data and transport code analyses?

The sensitivity of  $v_2$  to the assumed stiffness of the EOS was shown [8] to diminish rapidly below  $0.4A$  GeV and above  $6A$  GeV. We now tend to associate the weak sensitivity at low energies to the combined action of insufficient stopping [47] and still relatively modest compression. At energies well above  $4A$  GeV, on the other hand, the shadowing effect by spectator nucleons (and therefore the time clock) is no longer very effective as suggested by the observed sign change of  $v_2$  at  $4A$  GeV [51]. Presumably the spectator clock can be used to extend improved EOS constraints to densities (3-4  $\rho_0$ ) higher than was possible in the present work (limited to beams of  $1.5A$  GeV incident energy) in future accelerator systems such as FAIR in Darmstadt, Germany. However it is clear that beyond  $4A$  GeV, other ideas are needed to extract EOS information from heavy ion data.

As a main conclusion of the present work we believe we can say that the feasibility of establishing reasonably tight empirical constraints on the nuclear EOS has been demonstrated.

## Acknowledgments

This work was supported by the Helmholtz International Center for FAIR within the framework of the LOEWE program (Landesoffensive zur Entwicklung Wissenschaftlich-Ökonomischer Exzellenz) launched by the State of Hesse and under the contract number 13-70 by the German-French Exchange Program supported by GSI and IN2P3.

## References

### References

- [1] J. M. Lattimer, Ann. Rev. Nucl. Part. Sci. 62 (2012) 485.
- [2] A. Burrows, Rev. Mod. Phys. 85 (2013) 245.
- [3] A. Gezerlis, I. Tews, E. Epelbaum, S. Gandolfi, K. Hebeler, A. Nogga, A. Schwenk, Phys. Rev. Lett. 111 (2013) 032501
- [4] R. Machleidt, D. E. Entem, Phys. Rep. 503 (2011) 1; R. Machleidt, arXiv 1308.0103.
- [5] J. M. Lattimer, A. W. Steiner, Eur. Phys. J. A 50 (2014) 40.
- [6] J. Antoniadis et al., Science 340 (2013) 1233232.
- [7] P. B. Demorest, T. Pennucci, S. M. Ransom, M. S. E. Roberts, J. W. T. Hessels, Nature 467 (2010) 1081.
- [8] P. Danielewicz, R. Lacey, W. G. Lynch, Science 298 (2002) 1592.
- [9] R.B. Clare, D. Strottman, Phys. Rep. 141 (1986) 177.
- [10] A. Hombach, W. Cassing, S. Teis, U. Mosel Eur. Phys. J. A. 5 (1999) 157.

- [11] J.-Y. Ollitrault Phys. Rev. D (1992) 229. R PRD46(92)229
- [12] R. Stock, Phys. Rep. 135 (1986) 259.
- [13] Zhigang Xiao, Bao-An Li, Lie-Wen Chen, Gao-Chan Yong, Ming Zhang, Phys. Rev. Lett. 102 (2009) 062502.
- [14] Zhao-Qing Feng, Gen-Ming Jin, Phys. Lett. B 683 (2010) 140.
- [15] J. Aichelin, C. M. Ko, Phys. Rev. Lett. 55 (1985) 2661.
- [16] C. Sturm et al. (KaoS Collaboration), Phys. Rev. Lett. 86 (2001) 39.
- [17] C. Fuchs, A. Faessler, E. Zabrodin, Y. M. Zheng, Phys. Rev. Lett. 86 (2001) 1974; C. Fuchs, A. Faessler, S. El-Basaouny, E. Zabrodin, J. Phys. G 28 (2002) 1615; C. Fuchs, Prog. Part. Nucl. Phys. 56 (2006) 1.
- [18] Ch. Hartnack, J. Aichelin, J. Phys. G 28 (2002) 1649; Ch. Hartnack, H. Oeschler and J. Aichelin, Phys. Rev. Lett. 96 (2006) 012302; Ch. Hartnack, H. Oeschler, Y. Leifels, E. Bratkovskaya, J. Aichelin, Phys. Rep. 510 (2012) 119.
- [19] S. Wang et al., (EoS Collaboration), Phys. Rev. Lett. /6 (1996) 3911.
- [20] G. Peilert et al., Phys. Rev. 39 (1989) 1402. .
- [21] A. Andronic, et al. (FOPI Collaboration), Phys. Lett. B 612 (2005) 173.
- [22] W. Reisdorf, et al. (FOPI Collaboration), Nucl. Phys. A 876 (2012) 1, arXiv:1112.3180.
- [23] J. Aichelin, Phys. Rep. 202 (1991) 233.
- [24] C. Hartnack, et al., Eur. Phys. J. A 1 (1998) 151.
- [25] H. A. Gustafsson, et al., Phys. Rev. Lett. 52 (1984) 1590.
- [26] R. E. Renfordt, et al., Phys. Rev. Lett. 53 (1984) 763.
- [27] A. M. Poskanzer and S. A. Voloshin, Phys. Rev. C 58 (1998) 1671.
- [28] S. Voloshin, Y. Zhang, Zeitsch. Phys. C (1996) 665.
- [29] P. Danielewicz, G. Odyniec, Phys. Lett. B 157 (1985) 168.
- [30] H. Stöcker, et al., Phys. Rev. C 25 (1982) 1873.
- [31] G. Stoicea, et al., (FOPI Collaboration), Phys. Rev. Lett. 92 (2004) 072303.
- [32] J.-P. Blaizot, Phys. Rep. 64 (1980) 171.
- [33] E. Khan, J. Margueron, I. Vidaña, Phys. Rev. Lett. 109 (2012) 092501, E. Khan, J. Margueron, Phys. Rev. C 88 (2013) 034319.
- [34] M. Dutra, O. Lourenço, J. S. S a Martins, A. Delfino, J. R. Stone, P. D. Stevenson, Phys. Rev. C 85 (2012) 035201.

- [35] G. Taranto, M. Baldo, G. F. Burgio, Phys. Rev. 87 (2013) 045803.
- [36] T. Katayama, K. Saito, Phys. Rev. C 88 (2013) 035805.
- [37] F. Sammarruca, B. Chen, L. Corragio, N.Itaco, R. Machleidt, Phys. Rev. C86 (2012) 054317.
- [38] S. Fritsch, N. Kaiser, W. Weise, Nucl. Phys. A 750 (2005) 259.
- [39] R. Brockmann, R. Machleidt, Phys. Rev. C 42 (1990) 1965.
- [40] R. J. Furnstahl, K. Hebeler, arXiv:1305.3800
- [41] K. Hebeler, S. K. Bogner, R. J. Furnstahl, A. Nogga, A. Schwenk, Phys. Rev. C 83 (2011) 031301().
- [42] P. Moeller, W. D. Myers, H. Sagawa, S. Yoshida, Phys. Rev. Lett. 108 (2012) 052501.,
- [43] M. B. Tsang et al., Phys. Rev. C 86 (2012) 015803
- [44] R. Machleidt, arXiv 0710.2940 [nucl-th]
- [45] C. Fuchs, T. Gaitanos, Nucl. Phys. A 714 (2003) 643.
- [46] W. Reisdorf, et al. (FOPI Collaboration), Nucl. Phys. A 781 (2007) 459, arXiv: nucl-ex/0610025.
- [47] W. Reisdorf, et al. (FOPI Collaboration), Phys. Rev. Lett. 92 (2004) 232301.
- [48] W. Reisdorf, et al. (FOPI Collaboration), Nucl. Phys. A 848 (2010) 366, arXiv: nucl-ex/1005.3418.
- [49] H. H. Gutbrod, et al., Phys. Lett. B 216 (1989) 267.
- [50] H. H. Gutbrod, et al., Phys. Rev. C 42 (1990) 640.
- [51] C. Pinkenburg, et al. (E895 Collaboration), Phys. Rev. Lett. 83 (1999) 1295.
- [52] D. Brill et al., Z. Phys. A 355 (1996) 61.
- [53] P. Danielewicz, Nucl. Phys. A 673 (2000) 375.
- [54] E.E. Kolomeitsev et al., Workshop Trento 2004, J.Phys. G 31 (2005) 741; Workshop Trento 2009, unpublished.